Transient Control of Dynamic Inductive EV Charging and Impact on Energy Efficiency when Passing a Roadside Coil Section

[*]Giuseppe Guidi [*,†]Jon Are Suul,

*SINTEF Energy Research
7465 Trondheim, Norway
giuseppe.guidi@sintef.no

[†]Department of Engineering Cybernetics
Norwegian University of Science and Technology
7495 Trondheim, Norway

***Abstract*— This paper discusses the transient control of a system for dynamic inductive power transfer to an electric vehicle when passing a road-side coil section. A series-series-compensated topology with minimum number of passive components is assumed and a slight detuning of the resonance frequencies is introduced to limit the maximum induced current on the vehicle-side. A simple strategy for independent control of the road-side and vehicle-side coils is presented for ensuring strictly controlled charging power. The dynamic response of the resonant currents and of the power transfer is assessed by a small-scale experimental setup designed to represent a freight truck in scale 1:14. Experimental evaluation of the energy transfer efficiency is performed for high and low vehicle speeds and with different strategies for activating the control loops. The results demonstrate that the proposed strategy can ensure very short initialization transients and close-to-optimal operation at rated power when the vehicle-side coil is passing above the road-side coil, even at relatively high traveling speed. The concept of road utilization ratio is introduced to quantify the effect of length and layout of the road coil sections, as well as the dynamic transients, on the energy transfer capability of the system.**

Keywords—Energy Efficiency, Dynamic Inductive Power Transfer, Roadway-powered Electric Vehicles, Transient Control

I. INTRODUCTION

Significant progress in application of Inductive Power Transfer (IPT) technology for dynamic charging of Roadway-Powered Electric Vehicles (RPEVs) has been achieved during the last decade. Diverse development efforts have resulted in several different concepts for IPT-based RPEV systems being proposed and demonstrated [1]-[4]. The electromagnetic design of the coils for obtaining high power transfer efficiency and tolerance to misalignment have been critical challenges for this development, and several different concepts have been proposed [1], [2].

This work was partly supported by the project "Electric Infrastructure for Goods Transportation" (ElinGO - https://www.sintef.no/projectweb/elingo/), within the EnergiX program of the Research Council of Norway, and partly by the Internal Strategic Institute Project "Innovative Power Transfer Transfer Technology for Electric Transportation (IPT-ElTra) financed by the national Basic Funding Scheme of Norway.

In general, RPEV systems with very long road-side coil sections are expected to result in reduced efficiency due to the large magnetized road area which is causing high conduction losses. However, systems relying on many short road-side coils imply the need for a higher number of power electronic converters for controlling the system. The transition of a vehicle between adjacent sections of the road-side coil can also imply points of zero power transfer capability unless additional winding structures are included in the road-side or vehicle-side systems. Thus, attempts have been made to optimize the length of the road-side coil sections depending on the speed of the vehicles travelling on the road [5]. Design approaches for avoiding or limiting the power pulsations when passing the road-side coil sections have also been proposed [6]-[8]. However, less attention has been devoted to active control of the electrical transients of the road-side and vehicles side coils when a RPEV is entering and leaving each road-side coil section.

In this paper a simple control strategy is presented for energizing the road-side coil and activating the power transfer to a vehicle when it is entering a coil section along the road. The presented strategy is developed for a series-series compensated IPT topology with a slight detuning of the resonance frequencies, and ensures safe operation without any communication between the road-side and vehicle side control loops. Results obtained from a small-scale prototype designed for representing a heavy-duty freight truck, modelled in a scale of 1:14, demonstrates how the transient response depends on the vehicle position when the control sequence is activated. The road utilization ratio is introduced as a performance indicator for evaluating how the length of the road-side coil sections and the transients of the control strategy influence the energy transfer capability of an RPEV system.

II. SYSTEM TOPOLOGY AND CONTROL SYSTEM

A RPEV system configuration as shown in Fig. 1 is assumed, with center-pole road-side coils that are at least two times longer than the square-shaped vehicle-side coil. As shown in the figure, the length of one coil section is defined as l_{sect}, while the sections-to-section distance between two coils is l_{ss}. The road-side and vehicle-side coils have the same width,

This is the accepted version of a paper published in 2018 IEEE PELS Workshop on Emerging Technologies: Wireless Power - WoW 2018
DOI: 10.1109/WoW.2018.8450893

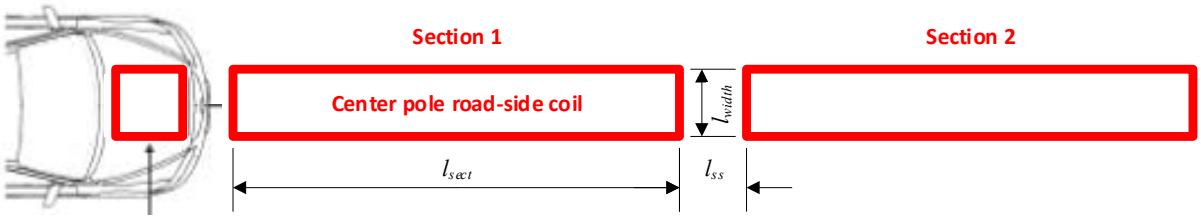

Fig. 1. RPEV travelling along a road with center-pole road-side coil sections

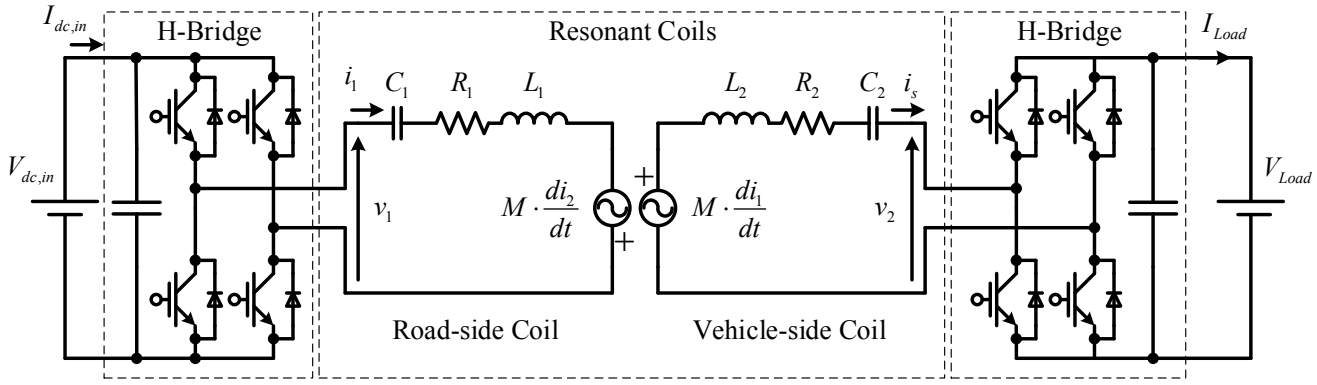

Fig. 2. Assumed topology for dynamic IPT system

l_{width}, which is assumed equal to the length of the vehicle-side coil.

As shown for one coil section in Fig. 2, a series-series (SS) compensated resonant topology with H-bridge converters on both sides is assumed. This topology is selected since it ensures the minimum number of passive components, thus avoiding unnecessary cost and reducing conduction losses to a minimum. Using an on-board active rectifier to control the power supplied to the load can also potentially result in higher on-board power density than adding a dedicated DC/DC converter after a passive rectifier. The assumed topology will also allow for bidirectional power flow [9], [10].

A. Characteristics of SS-compensated topology at resonance

When the system of Fig. 2 is ideally tuned, the unique resonant frequency of the system is defined as:

$$\omega_0 = \omega_{0,1} = \frac{1}{\sqrt{L_1 C_1}} = \omega_{0,2} = \frac{1}{\sqrt{L_2 C_2}} \tag{1}$$

Applying the harmonic approximation and assuming unity power factor at the receiving end, the coil currents at the resonant frequency can be expressed in terms of the terminal voltages as:

$$I_{1,res} = \frac{V_1 \cdot R_2 + V_2 \cdot \omega_0 M}{R_1 R_2 + \omega_0^2 M^2}; \quad I_{2,res} = \frac{V_1 \cdot \omega_0 M - V_2 \cdot R_1}{R_1 R_2 + \omega_0^2 M^2} \tag{2}$$

In the ideal case of a lossless system, the coil currents and the power flow from the input to the output reduce to:

$$I_{1,id} = \frac{V_2}{\omega_0 M}; \quad I_{2,id} = \frac{V_1}{\omega_0 M}; \quad P_{id} = \frac{V_1 \cdot V_2}{\omega_0 M} \tag{3}$$

To better illustrate the intrinsic characteristics of the system, a suitable per-unit system is introduced. The voltages applied to the resonant coils are normalized to their maximum possible value according to the topology in Fig. 2:

$$v_x = \frac{V_x}{V_{N,x}}; \quad V_{N,x} = V_{dc,x} \cdot \frac{4}{\pi}; \quad with\ x = 1,2 \tag{4}$$

Defining the base power as the maximum power that will be transferred at the best possible coupling, the following base values are introduced for power, current and impedance, respectively:

$$P_N = \frac{V_{N,1} \cdot V_{N,2}}{\omega_0 M_{\max}}; \; I_{N,x} = \frac{2P_N}{V_{N,x}}; \; Z_{N,x} = \frac{V_{N,x}}{I_{N,x}} \quad with\ x = 1,2 \tag{5}$$

Moreover, the mutual inductance M is expressed in terms of the non-dimensional coupling coefficient k and the quality factor Q, as they are intrinsic characteristics of the system that are rather independent of scaling:

$$\begin{aligned} \omega \cdot m &= \frac{\omega M}{\sqrt{Z_{N1} \cdot Z_{N2}}} = r_{12} \cdot k \cdot Q; \\ r_{12} &= \sqrt{\frac{R_1}{Z_{N,1}} \cdot \frac{R_2}{Z_{N,2}}}; \quad Q = \sqrt{\frac{\omega L_1}{R_1} \cdot \frac{\omega L_2}{R_2}} \end{aligned} \tag{6}$$

Normalized currents in resonance are then expressed as:

$$i_1 = \frac{\frac{v_1}{r_1} + \frac{v_2}{r_{12}} \cdot kQ}{1 + (kQ)^2}; \quad i_2 = \frac{\frac{v_1}{r_{12}} \cdot kQ - \frac{v_2}{r_2}}{1 + (kQ)^2} \tag{7}$$

Note that both currents tend to 1.0 pu when rated power is being transferred at rated coupling, under the assumption of small losses ($kQ \gg 1$).

B. Detuning for improved secondary side short-circuit characteristics of SS-compensated topology

Since the control of the vehicle-side H-bridge in Fig. 2 needs to be synchronized the resonant current, it is convenient to let the converter output zero voltage at the start of the control sequence. Thus, it is particularly important to analyze

This is the accepted version of a paper published in 2018 IEEE PELS Workshop on Emerging Technologies: Wireless Power - WoW 2018
DOI: 10.1109/WoW.2018.8450893

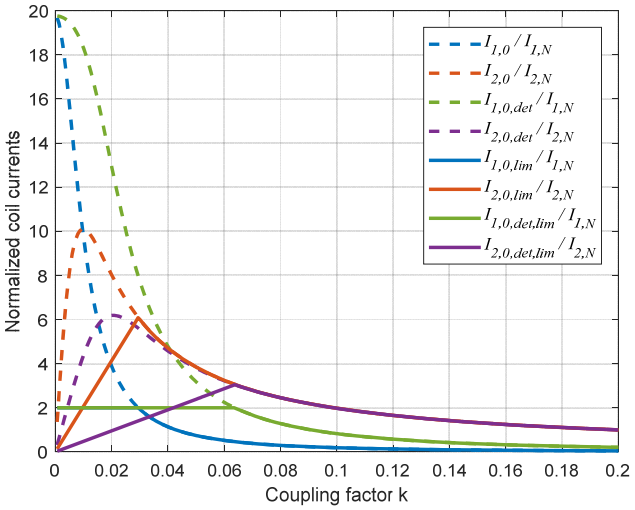

Fig. 3. Normalized coil currents as function of coupling factor for short-circuited on-board coil (Q = 100, $r_1 = r_2$ = 0.05 pu).

the currents in the coils for the expected range of coupling conditions when the on-board coil terminals are short-circuited.

Setting v_2 = 0 and v_1 = 1 pu in (7), the maximum short-circuit currents can be evaluated as function of the coupling coefficient, as shown by the dashed blue and red lines in Fig. 3 when assuming Q to be constant. This condition approximates the dynamic situation of a vehicle approaching an energized track with its on-board coil short-circuited and with full voltage applied to the road-side coil. As expected, current on both sides of the coil grows to several times the rated current for small values of coupling.

Since the road-side coil is fed via a power converter, it is relatively easy to control v_1 so that i_1 will not exceed a specified value. As an example, the solid blue and red lines in Fig. 3 show the situation when the road-side coil current is limited to 2.0 pu. The curves clearly show that limiting the current in the road-side coil to safe values does not prevent the induced current in the vehicle-side coil to raise excessively. In the presented example, more than 6.0 pu of current is calculated for the worst-case coupling. Similar (or even higher) worst-case current will be observed in any practical systems designed for high efficiency at rated power transfer.

As illustrated by the results in Fig. 3, significant oversizing of the on-board converter would be needed to withstand the worst-case short-circuit currents on the vehicle-side, even if the road-side currents are appropriately limited. Alternatively, very quick and reliable communication must be in place to allow for control of the on-board induced current via the road-side converter. Clearly, none of those solutions are desirable for a simple and reliable system.

However, as will be demonstrated, the worst-case induced current can be drastically reduced by applying the design method proposed in [11], [12], originally intended for reducing switching losses of the road-side converter. This design approach is based on deliberately detuning the resonance frequencies of the coils according to a factor:

$$x_c = \frac{C_1 \cdot L_1}{C_2 \cdot L_2} > 1 \tag{8}$$

The analytical expression of the coil current for the general case of $x_c \neq 1$ is rather complex and is not reported here due to space limitations. However, the solution for x_c = 1.05 is shown by the green and violet lines in Fig. 3. While this very moderate detuning has virtually no effect on the nominal power transfer, as verified in [12], the worst-case induced current is reduced from more than 6.0 to less than 3.0 pu. The effect would be even higher if more detuning is introduced. Furthermore, the detuning ensures that a given current limitation for the road-side coil will be active for a wider range of coupling conditions. Thus, as shown by the solid green and violet curves in Fig. 3, the detuning ensures that the vehicle-side short circuit current can more effectively limited by limiting the road-side currents. This observation opens the possibility of using simple operational strategies with independent control of the road-side and vehicle side converters of the SS-compensated dynamic IPT system.

C. *Independent control of road-side and vechile-side coils*

The relatively low induced current ensured by the proposed detuning could make it possible to keep the road-side coil energized at all time, as long as its current is limited to a safe value. However, to avoid unnecessary losses, the operational strategy is modified as described in the following:

1) Road-side control

According to the state-machine sketched in Fig. 4, the road-side coil section is only energized when an approaching vehicle is detected. As soon as the vehicle is detected at a specific position, the current in the road-side coil is controlled and limited below a constant reference value. As shown in Fig. 5, the current is regulated by a PI-controller providing a voltage reference for the phase-shift modulation of the road-side H-bridge converter [9]. The road-side converter is turned off as soon as the vehicle is detected to leave the coil section.

2) Vehicle-side control

For the vehicle-side coil, the control sequence is slightly more complicated, since the rectifier is an actively controlled H-bridge, implying that the control system must be synchronized to the resonant current to be able to control the power received by the load on-board the vehicle. As mentioned in section II-B, the vehicle-side H-bridge converter is outputting zero voltage and the coil is effectively short-circuited during idle operation. Thus, current will start to flow when there is non-negligible coupling with an energized road-side coil section. The Phase Locked Loop (PLL) of Fig. 6 is utilized for synchronizing the H-Bridge modulator to the resonant current, and the load current control is a simple PI-controller providing the voltage reference for the phase-shift modulation of the vehicle-side H-bridge, as shown in Fig. 7. As indicated in Fig. 6, the PLL is based on comparison of the zero-crossing of the coil current with the saw-tooth carrier used by the phase-shift modulator of the H-bridge.

The control of the load current can be activated when the PLL is locked to the frequency and phase angle of the resonant current. Similarly, the load current control will be deactivated if the PLL loses synchronization due to low coupling or if the road-side converter is turned off. The structure of the state machine controlling the operation of the vehicle-side converter is shown in Fig. 8.

This is the accepted version of a paper published in 2018 IEEE PELS Workshop on Emerging Technologies: Wireless Power - WoW 2018
DOI: 10.1109/WoW.2018.8450893

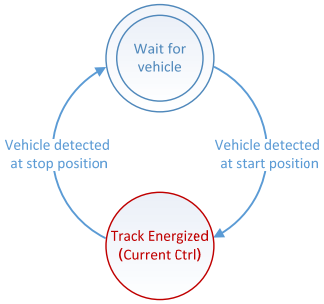

Fig. 4. State machine for road-side control

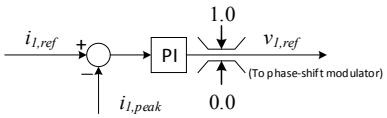

Fig. 5. Current control of road-side coil

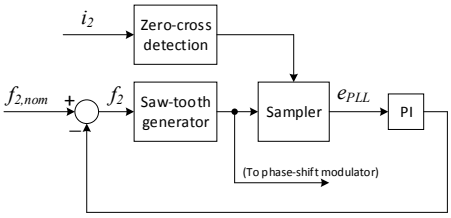

Fig. 6. Phase Locked Loop for synchronizing the vehicle-side control to the resonant current

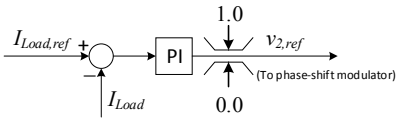

Fig. 7. Current control of vehicle-side coil

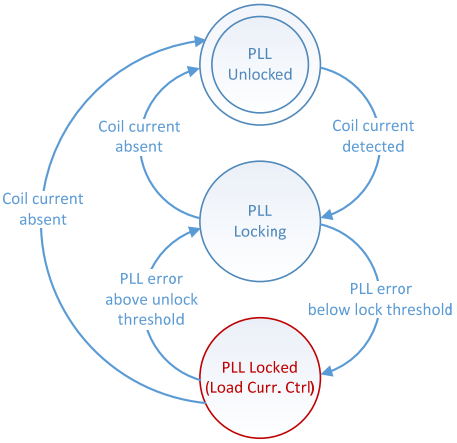

Fig. 8. State machine for vehicle-side control

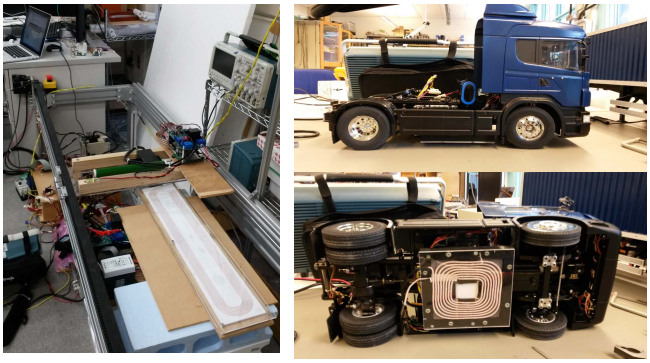

Fig. 9. Test track with road-side coil and servo-controlled sliding pick-up; Pickup coil mounted on vehicle

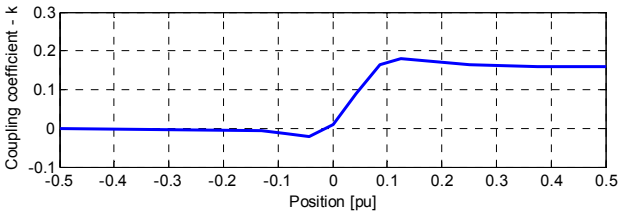

Fig. 10. Coupling characteristics as function of position, in case of perfect alignment in the direction orthogonal to travel.

III. Experimental Setup

A small-scale prototype designed for a 1:14 scale model of a heavy duty-freight truck has been constructed and used for testing the presented system design and the applied control strategy by assessing the operation at different speeds. Pictures of the coils are shown in Fig. 9, where the road-side coil is shown to the left when mounted on a servo-controlled rail for accurate testing of the system characteristics. The vehicle-side coil is shown on the right-hand side as mounted on the truck model. The main parameters of the coils are listed in Table I. Note that the IPT coils have been designed with a relatively high detuning factor x_c equal to 1.1, to allow for excitation of the road-side coil at any coupling factor with the vehicle-side coil without risk of excessive induced current.

The truck model is equipped with a 7.4V, 5.5 Ah Lithium Polymer battery representing the load of the IPT system. For simplicity, identical H-bridges are used for the road-side and vehicle-side converters. The H-bridges are based on conventional low voltage Si-MOSFETs (IRFR7440). Custom-made control boards, based on Xilinx Zynq System-On-Chip are used on both sides to implement the proposed control strategies.

TABLE I PARAMETERS OF SMALL-SCALE TEST SYSTEM

Nominal power, P_0	40 W
I/O voltages, $V_{dc,in}$ $V_{dc,out}$	12.0 V, 7.4 V
Road-side coil	
Planar dimensions	570 mm by 100 mm
Self-inductance (with no pick-up), L_1,	36.7 μH
Resonance frequency (with no pick-up)	74 kHz
Measured resistance (at 75 kHz)	128 mΩ,
Vehicle-side coil	
Planar dimensions	100 mm by 100 mm
Self-inductance (above road-side coil), L_2,	8.3 μH
Resonance frequency (above road-side coil)	78 kHz
Measured resistance (at 75 kHz)	65 mΩ,
Coupling conditions	
Airgap distance	22 mm
Coupling factor, k (centered, max coupling)	0.16, 0.18
Detuning factor x_c	1.1

The coupling coefficient obtained from Finite Element Method (FEM) analysis of a single road-side coil as a function of the vehicle-side coil position is shown in Fig. 10. In this figure, the zero position corresponds to the null-point, where the coupling between the two coils is zero, while 1.0 pu corresponds to the length of the road-side coil. As seen from the figure, there is a region with a small negative coupling when the vehicle-side coil is approaching the road-side section. After the vehicle-side coil reaches the null-point, the coupling increases rapidly to a maximum value of about 0.18, before it reduces slightly towards 0.16 when the vehicle-side coil is approaching the middle of the road-side coil.

IV. Experimental Results

The operational strategy proposed in section II.C has been tested with three different conditions for activating the control of the road-side coil (TX). As illustrated in Fig. 11, these three conditions correspond to activation of the road-side coil when the vehicle-side coil is one coil width before the null-point (i.e. 100 mm, position = −0.18 pu), at the null-point (position = 0.0 pu), or one coil width after the null-point (i.e. 100 mm,

This is the accepted version of a paper published in 2018 IEEE PELS Workshop on Emerging Technologies: Wireless Power - WoW 2018
DOI: 10.1109/WoW.2018.8450893

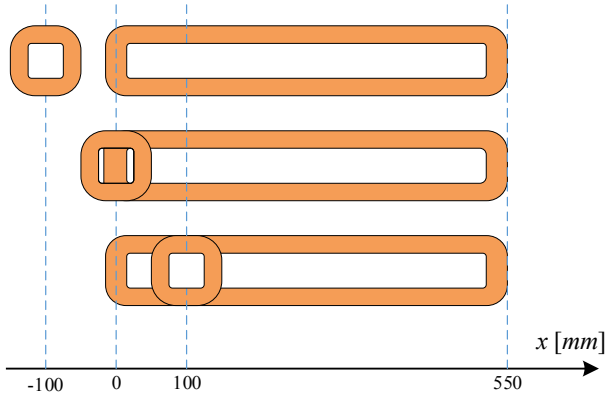

Fig. 11. Position of the vehicle-side coil for the three different investigated strategies for activating the control of the road-side coil

position = 0.18 pu). In all experiments the set-point for the charging current of the Li-Po battery is fixed to 5.5 A (1C), regardless of the battery voltage (CC charging mode).

A set of results obtained with controlled movement of the vehicle-side coil on the servo-controlled rail from Fig. 9 is shown in Fig. 12 a)-b) and c)-d) for two different speeds corresponding to 42.5 and 86 km/h for a full-scale vehicle (due to the scaling factor of 1:14).

In case of early activation of the road-side coil (black lines in Fig. 12), the converter starts operating when the coupling is very low, and the track current quickly rises to the specified limit of 10.0 A. Note that this limit corresponds to about 1.5 times the current of the road-side coil observed during rated power flow at maximum coupling. The induced current in the initially short-circuited on-board pickup coil is proportional to the coupling and remains small until the null-point is passed. After the null-point, the induced current rises quickly, allowing the PLL to lock and the charging current control to be activated. Note that the peak value of the induced current during the short-circuited start-up phase is only about 1.75 times the coil current observed when rated power is flowing at the maximum coupling. After the on-board converter is activated, the charging current is immediately controlled to the set-point and the change in coupling coefficient due to

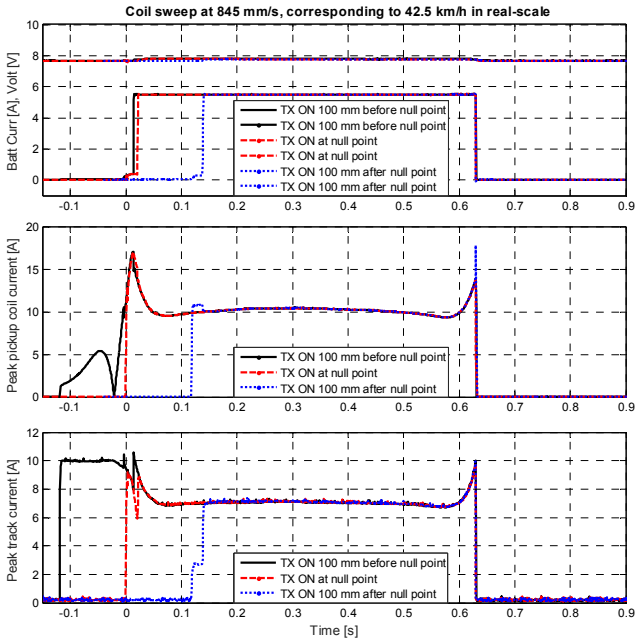

a) Resonant currents at low speed

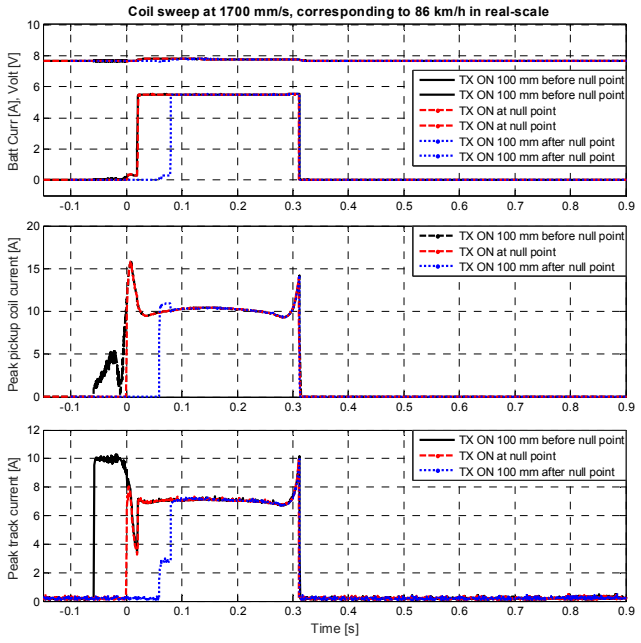

c) Resonant currents at high speed

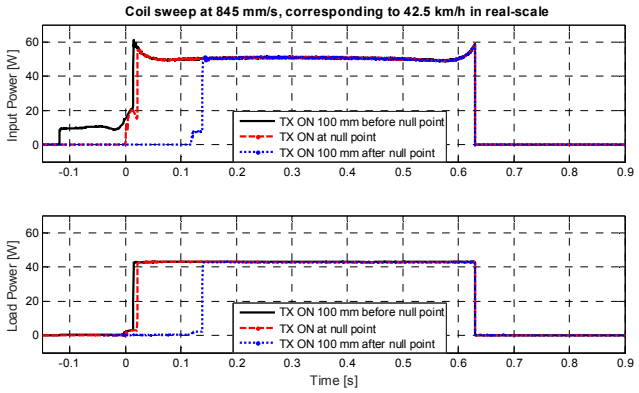

b) Power flow at low speed

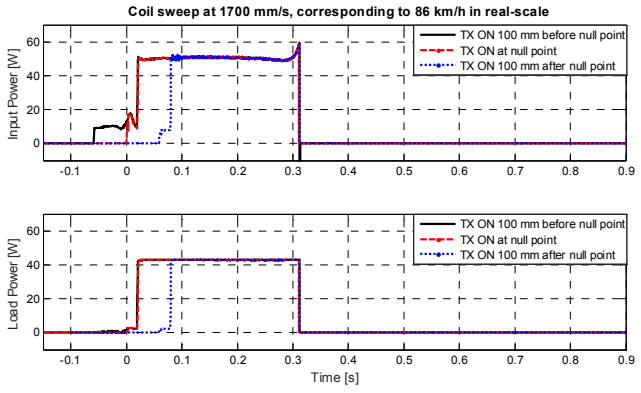

d) Power flow at high speed

Fig. 12. Experimental results obtained at two different speeds with energization of the road-side coil at different positions of the vehicle

This is the accepted version of a paper published in 2018 IEEE PELS Workshop on Emerging Technologies: Wireless Power - WoW 2018
DOI: 10.1109/WoW.2018.8450893

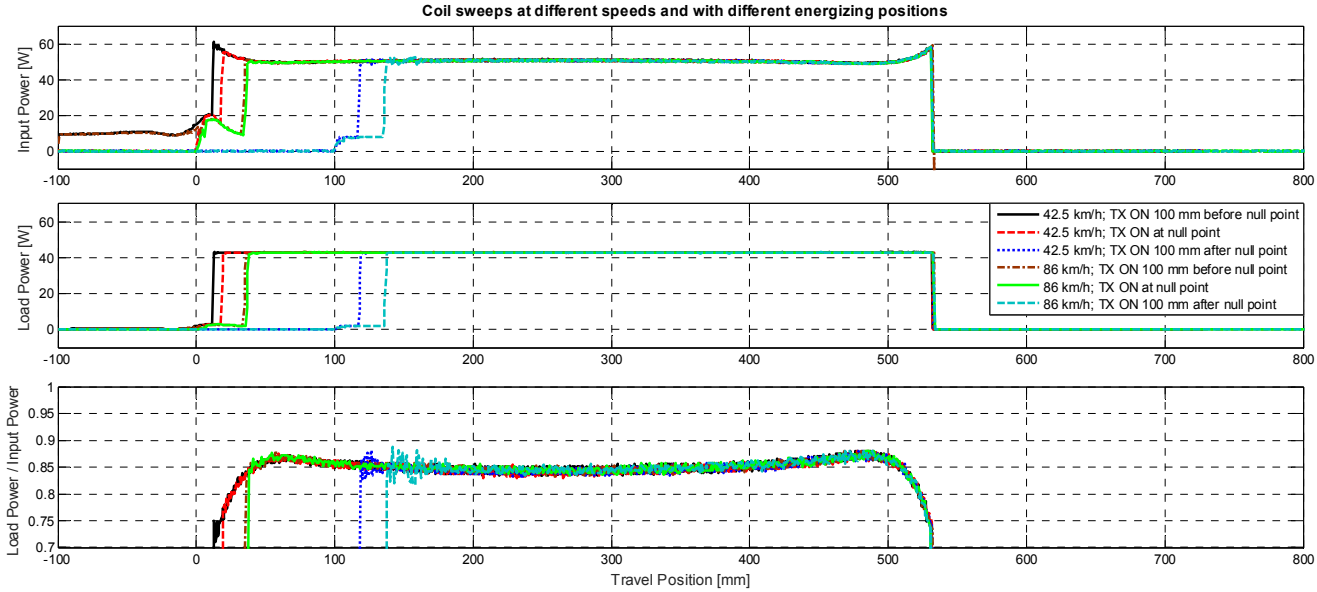

Fig. 13. Input power, output power, and their ratio as a function of the vehicle-side coil position

movement along the road-side coil is completely rejected by the controller.

In case the road-side coil is activated at the null-point (red lines in Fig. 12), the initial phase characterized by limited track current and no power transfer is completely avoided. The PLL locking and power transfer phases are very similar to the previous case, suggesting that the approximately same amount of energy is transferred to the load.

If the activation of the road-side coil is delayed (blue lines in Fig. 12), the transient response is slightly different, since the coupling is already high when the control sequence is activated. The short-circuit current of the pickup coil is almost the same as the rated current, while the track current is rather low, as predicted by Fig. 3. The PLL locking time is clearly visible in the figure, as it is the time from the step of the on-board coil current due to track activation to the step of the battery current when the load current regulator is activated. It is apparent that the PLL locking time is much longer than the response time of the load current regulator.

The measured power flow at the input to the system and the power supplied to the battery are shown in Fig. 12 b) and d) for the two different speeds. From these figures, it can be clearly seen that if the road-side coil is energized after the null-point, the transient response can be very quick and smooth, but a noticeable delay appears before the power transfer can start. This effect is visible at all speeds, but increases at high speed as can be seen from Fig. 12 d), where a larger share of the active power transfer interval is lost due to the delayed start. Thus, the suggested strategy is to activate the road-side coil when the vehicle-side coil is passing the null-point.

The power supplied to the road-side coil and the power transferred to the load, as well as the ratio between these two power measurements, is plotted in Fig. 13 as a function of the position of the vehicle-side pickup coil for all the cases in Fig. 12. The figure shows that the power ratio when the system is in operation is the same at any position for all the cases. This implies that that the energy storage capacity of the reactive components of the IPT system has negligible influence on the energy transfer. Thus, the power ratio is approximately equal to the instantaneous efficiency, in the same way as for a power conversion process without internal energy storage components. From this result it can also be inferred that the efficiency of the system is independent of the motion. In other words, the dynamic transfer process has the same instantaneous efficiency as a hypothetical system for static power transfer operating at the same coupling conditions.

From the results presented in Fig. 12 and Fig. 13, it can be seen that the total energy transfer from the road-side infrastructure to a vehicle when passing one coil section is strongly influenced by the speed and by the strategy for activating the control sequence. A numerical evaluation of the energy transfer obtained from the experimental results is also given in Table II. In this table, the energy "E_2" is the total energy transferred to the load, which is calculated as the integral over time of the measured load power from Fig. 12. Obviously, the higher the speed, the lower the energy that can be transferred to the battery in the event of passing a single road-side coil. Indeed, the maximum power flow is constant and the time available for transferring energy from a single road-side coil is inversely proportional to speed. As expected, the amount of energy transferred to the battery is essentially the same for the cases of early activation and for null-point activation of the road-side coil, while it is noticeably reduced in case of delayed activation. The "loss" of charging energy due to late activation of the road-side coil becomes more noticeable as the speed increases. About 20% of the energy transfer potential is lost at the highest speed tested.

The energy transfer efficiency η_E is also listed in Table II for all the presented cases. These values are obtained as the ratio between the energy transferred to the load and the energy supplied to the road-side coil (i.e. the integral of the measured power supplied to the road-side coil). The cases corresponding to early activation of the road-side coil yield the lowest energy efficiency. This is mainly due to the losses occurring in the system when the road-side coil is magnetized without

This is the accepted version of a paper published in 2018 IEEE PELS Workshop on Emerging Technologies: Wireless Power - WoW 2018
DOI: 10.1109/WoW.2018.8450893

TABLE II ENERGY TRANSFER EFFICIENCY AND ROAD UTILIZATION RATIO

$v_{vehicle}$	845 mm/s (42.5 km/h)			1700 mm/s (86 km/h)		
TX activation point $[mm]$	-100 (early)	0 (null-pt)	+100 (late)	-100 (early)	0 (null-pt)	+100 (late)
$E_2[J]$	26.6	26.2	21.2	12.7	12.6	10.0
η_E	0.81	0.84	0.85	0.81	0.84	0.84
$u_{road}(l_{sect}, 50mm)$	0.84	0.83	0.67	0.82	0.81	0.64
$u_{road}(l_{sect}, 0)$	0.92	0.91	0.73	0.89	0.88	0.70

transferring any power to the load. For all activation strategies, the energy transfer efficiency is almost independent of the travelling speed.

The last two rows of Table II show the road utilization ratio u_{road}, which is introduced as a performance indicator for evaluating how the control strategy and the layout of the road-side coil sections influence the energy transfer efficiency of the system. Thus, u_{road} is defined as the ratio between the actual energy transferred to the load and the energy that would be transferred in case of an ideal continuous rail allowing for constant power transfer equal to the power reference independently of the position. Based on the general system layout sketched in Fig. 1, u_{road}, is expressed as:

$$u_{road}(l_{sect}, l_{ss}) = \frac{E_2(l_{sect})}{P_{chg,ref} \cdot \frac{l_{sect} + l_{ss}}{v_{vehicle}}} < 1 \qquad (9)$$

where $P_{chg,ref}$ is the charging power reference (charging current reference multiplied by the battery voltage, in case of CC charging), $v_{vehicle}$ is the speed of the vehicle and l_{sect}, l_{ss} are defined in Fig. 1.

The ratio in (9) also gives a measure of the necessary oversizing of the power rating of a given system layout, due to loss of power transfer resulting from road-coil sectioning and from non-ideal dynamic response. The quantity u_{road} (l_{sect},0) indicates the effect of the dynamic control response only.

From the results in Table II, it can be noticed that the road utilization ratio is only marginally affected by the vehicle speed, while it is rather sensitive to the spacing between adjacent road-side coil sections. Most importantly, delayed activation of the road coil leads to poor utilization of the road-side infrastructure, especially at high speed.

V. CONCLUSION

The control sequence and transient response of a dynamic IPT system for RPEVs has been investigated when a vehicle is passing a road-side coil section. A simple design strategy for avoiding high induced currents during transients and a corresponding control system for ensuring safe magnetization of the road-side coil and accurate control of the charging power to the on-board load was also presented. Based on results from a small laboratory model in scale 1:14, it has been demonstrated that the road-side coil should be energized when the vehicle-side coil is close to the null-point of the coupling with the vehicle-side coil. In this case, the lost energy due to the initial transients is marginal, and the energy transfer efficiency of the system can be maintained high, even with relatively high vehicle speeds. However, at high speeds, the average power transfer capability during the time it takes to pass one road-side coil section will become more sensitive to the delay caused by the control sequence for initiating the power transfer to the vehicle. Thus, the importance of a fast response of the control system will increase at high speeds. The road utilization ratio has been introduced for quantifying the effect of the road-side coil layout and of non-ideal dynamic response of the control system when passing a road-side coil section. This ratio can be used as a performance indicator for comparing the impact of different system designs and control strategies on the average power transfer capability to the vehicle.

REFERENCES

[1] S. Y. Choi, B. W. Gu, S. Y. Jeong, C. T. Rim, "Advances in Wireless Power Transfer Systems for Roadway-Powered Electric Vehicles," in *IEEE Journal of Emerging and Selected Topics in Power Electronics*, Vol. 3, No, 1, March 2015, pp. 18-36

[2] C. C. Mi, G. Buja, S. Y. Choi, C. T. Rim, "Modern Advances in Wireless Power Transfer Systems for Roadway Powered Vehicles," in *IEEE Transactions on Industrial Electronics*, Vol. 63, No. 10, October 2016, pp. 6533-6545

[3] N. P. Suh, D. H. Cho, Red. "The On-line Electric Vehicle – Wireless Electric Ground Transportation Systems," Springer, Cham, Switzerland, 2017

[4] C. T. Rim, C. Mi, Wireless Power Transfer for Electric Vehicles and Mobile Devices," Wiley, 2017

[5] W. Zhang, S.-C. Wong, C. K. Tse, Q. Chen, "An Optimized Track Lenght in Roadway Inductive Power Transfer Systems," in *IEEE Journal of Emerging and Selected Topics in Power Electronics*, Vol. 2, No. 3, September 2014, pp. 598-608

[6] F. Lu, H. Zhang, H. Hofmann, C. C. Mi, "A Dynamic Charging System With Reduced Output Power Pulsation for Electric Vehicles," in *IEEE Transactions on Industrial Electronics*, Vol. 63, No. 10, October 2016, pp. 6580-6590

[7] Y. Guo, Q. Zhu, C. Liao, F. Li, "Switch-On Modeling and Analysis of Dynamic Wireless Charging System Used for Electric Vehicles," in *IEEE Transactions on Industrial Electronics*, Vol. 63, No. 10, October 2016, pp. 6568-6579

[8] A. Ong, P. K. S. Jayathurathnage, J. H. Cheong, W. L. Goh, "Transmitter Pulsation Control for Dynamic Wireless Power Transfer Systems," in *IEEE Transactions on Transportation Electrification*, Vol. 3, No. 2, June 2017, pp. 418-426

[9] B. X. Nguyen, D. Mahinda, G. H. B. Foo, P. Wang, A. Ong, U. Madawala, T. D. Nguyen, "An Efficiency Optimization Scheme for Bidirectional Inductive Power Transfer Systems," in *IEEE Transactions on Power Electronics*, Vol. 30, No. 11, November 2015, pp. 6310-6319

[10] Z. U. Zahid, Z. M. Dalala, R. Chen, B. Chen, J.-S. Lai, "Design of Bidirectional DC-DC Resonant Converter for Vehicle-to-Grid (V2G) Applications," in *IEEE Transactions on Transportation Electrification*, Vol. 1, No. 3, October 2015, pp. 232-244

[11] G. Guidi, "An apparatus and a method for wireless transmission of power between DC Voltage sources," Norwegian Patent 341430, filed January 2015, granted November 2017

[12] G. Guidi, J. A. Suul, "Minimizing Converter Requirements of Inductive Power Transfer Systems with Constant Voltage Load and Variable Coupling Conditions," in *IEEE Transactions on Industrial Electronics*, Vol. 63, No. 11, November 2016, pp. 6835-6844

This is the accepted version of a paper published in 2018 IEEE PELS Workshop on Emerging Technologies: Wireless Power - WoW 2018
DOI: 10.1109/WoW.2018.8450893